# Stabilizing the NASICON Solid Electrolyte in an Inert Atmosphere as a Function of Physical Properties and Sintering Conditions for Solid-State Battery Fabrication

Hari Raj, Timothée Fabre, Marie Lachal, Audric Neveu, Justine Jean, Marlu César Steil, Renaud Bouchet, Valérie Pralong

# Stabilizing the NASICON solid electrolyte in inert atmosphere as a function of physical properties and sintering conditions for solid state battery fabrication

Hari Raj[1], Timothée Fabre[3], Marie Lachal[3], Audric Neveu[1], Justine Jean[1], Marlu César Steil[3], Renaud Bouchet[3], Valérie Pralong[1,2*]

[1]Normandie University, Ensicaen, Unicaen, CNRS, Crismat, 14000 Caen, France

[2]Réseau sur le Stockage Electrochimique de l'Énergie (RS2E), Amiens, France

[3]University Grenoble Alpes, Université Savoie Mont Blanc, CNRS, Grenoble INP, LEPMI, 38000 Grenoble, France

*Corresponding Author: valerie.pralong@ensicaen.fr

## Abstract

The interfacial contact between solid electrolyte and cathode materials is one of the challenges for solid state battery (SSB) industry. The co-sintering of solid electrolyte and cathode materials could be a possible solution. Considering the future scope of solid state battery fabrication by co-sintering process of phosphate based solid electrolyte and phosphate based cathodes ($LiFePO_4$, $Li_3V_2(PO_4)_3$ etc.), present study focuses on stabilizing the NASICON structured $Li_{1.4}Al_{0.4}Ti_{1.6}(PO_4)_3$ (LATP) solid electrolyte in inert atmosphere because proposed cathode materials are not stable in air at high temperature. The results show high influence of particle size and heating rate along with sintering temperature on achieving pure phase and fully dense pellets in argon atmosphere. The cracks/voids, secondary phases and reduction of Ti were observed in the

pellets prepared with powder of bigger size under the argon gas sintering. The present work does not only successfully solve these issues by decreasing particle size and reducing heating rate but also produces highly dense pellet with more than 98% density at 800 °C. We have also achieved high conductivity of $8.77\times10^{-4}$ S $cm^{-1}$ at room temperature for the pellet sintered at just 800 °C in argon which is 3 - 4 times higher than the conductivity of samples sintered at higher than 800 °C. Therefore, we succeed to obtain for the first time a high conductivity, pure phase and high density of the LATP solid electrolyte at relatively low temperature of 800 °C in argon atmosphere, which is an important solution for solid state battery fabrication by co-sintering process. Furthermore, the stabilized NASICON electrolyte in argon atmosphere also shows superior electrochemical performance when tested with Li metal in symmetric battery cell.

**Keywords:** Solid state batteries; NASICON; X-ray diffractometer; Li-ion diffusion; LATP.

## Introduction

Conventional Li-ion batteries (LIBs) have been covered wide area of applications from portable electronics to electric vehicles as a major energy source. However, current LiBs are facing challenges to fulfil the safety, high energy and power demands of fast-growing market of electric vehicles (EVs) and hybrid electronic vehicles (HEVs) [1 - 4]. In particular, liquid organic electrolytes used in conventional LIBs have raised the safety issues due to serious fire risk because of its flammability and volatility [5, 6]. The battery scientist community has proposed solid-state batteries (SSBs) as a replacement of current LIBs, which have the potential to overcome most of the prevailing problems associated with LIBs. Therefore, extensive research is being focused to replace liquid electrolyte with suitable solid electrolyte for next-generation (SSBs) [1, 2, 7].

The inorganic solid electrolytes are well-known for their realistic industrial manufacturing due to higher stability against ambient air and high temperature [8, 9]. In general, inorganic solid electrolytes can be categorized in different groups such as oxides (perovskite, garnet), phosphates (NASICON), sulfides, hydrides, halides and glasses [10]. Among the above stated solid electrolytes, oxides and phosphates have advantage over others due to higher mechanical strength and Li-ion conductivity in the range of $10^{-3}$ - $10^{-5}$ S $cm^{-1}$ [11]. In general, it is considered that, for practical applications, a solid electrolyte should have Li-ion conductivity at least in the order of $10^{-4}$ S $cm^{-1}$ [12].

The NASICON type $LiTi_2(PO_4)_3$ (LTP) has shown very promising properties in terms of chemical/thermal stability and low cost. However, LTP suffers with poor total ionic conductivity in the range of $10^{-8}$ to $10^{-6}$ S $cm^{-1}$ at room temperature [13-15]. The doping of Al in LTP has increased its ionic conductivity many folds with the compound known as $Li_{1+x}Al_xTi_{2-x}(PO_4)_3$ (LATP) [16]. The ionic conductivity of LATP has been reported up to $10^{-4}$ to $10^{-3}$ S $cm^{-1}$ at room

temperature [17]. The conductivity of LATP depends on many factors such as doping level of Al [18-20], density of sintered LATP [11, 21-24], sintering temperature [11, 22, 25], secondary phases present in the sample [22-24, 26], microstructure of sintered LATP [11, 22, 25-28], synthesis method [11, 17, 20, 22] etc. However, in above mentioned studies on LATP solid electrolytes, sintering was performed in air or oxygen environment [11, 16-28].

If fabrication of SSB is considered by co-sintering process of LATP solid electrolyte and phosphate based cathode materials such as $LiFePO_4$, $Li_3V_2(PO_4)_3$, sintering can only be possible in inert atmosphere ($Ar/N_2$) because these cathode materials are not stable in air at high temperature. Furthermore, study of sintering behavior of LATP in inert atmosphere can play an important role in SSB fabrication by co-sintering process with $LiFePO_4$ and $Li_3V_2(PO_4)_3$ cathodes.

Therefore, by considering more practical approach for SSB fabrication through co-sintering process, present work focuses on sintering behavior of $Li_{1.4}Al_{0.4}Ti_{1.6}(PO_4)_3$ solid electrolyte in argon (Ar) atmosphere as a function of particle size and sintering conditions. The comparative study is also done with LATP sintered in air.

## Experimental Section

The solid electrolyte material $Li_{1.4}Al_{0.4}Ti_{1.6}(PO_4)_3$ (LATP) was purchased from NEI Corporation. The structural analysis was done by X-ray diffractometer (Philips X'Pert) using Cu-$K_\alpha$ (1.54Å) radiation in the 2θ range of 10°-90° with step size of 0.013°. The qualitative phase analysis was carried out using X'Pert HighScore Plus software on the basis of the powder diffraction file (PDF) database and the inorganic crystal structure database (ICSD).

Particle size analysis was carried out by Granulometry (Mastersizer 2000, Germany) using ethanol as dispersant media. The dilatometry analysis (Setsys 16/18, SETARAM) was performed to

determine the linear change in the pellets as a function of temperature in the air and argon atmospheres. LATP powder was pre-heated at 450 °C for 3h in air before characterization to remove any traced industrial organic impurities, confirmed by TG analysis (supporting information Fig. S1).

The LATP powder was pressed into pellets of 10 mm diameter using by uniaxial press with 3.0 ton of pressure. The sintering of pellets was carried out on $Al_2O_3$ crucible at different temperatures under Air/Argon environments. The dwell time was kept 2h for all experiments, however, variable heating rate was used to get optimize conditions i.e. low reactivity and high density.

Ball milling of procured LATP powder was carried out using planetary milling (Fritsh), and $ZrO_2$ jar (25 ml) & balls ($\Phi$ = 3.0 mm) for 2h at 400 RPM in isopropyl alcohol (IPA) wet media. The ball milled powder samples of LATP were named as LATPBM. Microstructures of powders and sintered pellets were determined by scanning electron microscopy (ZEISS Supra55 FEG). The sintered pellets were cut into half to determine the microstructures of cross-section area which provides information of sintering behavior internally.

For AC impedance spectroscopy measurement, sintered pellets were polished and coated with Pt on both sides for preparing blocking cell (Pt/LATP/Pt). The BioLogic Controlled Environment Sample Holder (CESH) was used to hold the sample, and BioLogic VMP3 analyzer was used to apply a signal of frequency from 1.0 MHz to 0.1 Hz with an amplitude of 50 mV. The measurement was carried out in the temperature range of -40 °C to 80 °C controlled by the BioLogic Intermediate Temperature System (ITS). The samples were placed inside the holder in air before closing the CESH holder. Therefore, all measurements were carried out in Air. The measured impedance spectra (Nyquist plots) were fitted to an appropriate electrical equivalent circuit $[R_1+(R_2 \| Q_1)+Q_2]$ for all samples by least squares method using Z-fit Ec-Lab software. The total conductivity was

calculated from resistance R determined from fitting of Nyquist plot and geometry of the pellets. The following formula was used for determining the conductivity: $\sigma = \frac{1}{R}\frac{l}{A}$; where, *R* is resistance, and *l* and *A* are thickness and area of pellet, respectively [24].

Electrochemical study of sintered pellets was done in symmetric cells configuration with Li-metal by using BioLogic VMP3 analyzer at different current densities. Before the electrochemical test, pellets were polished to reduce the thickness and making smooth surface for better interface between solid electrolyte and Li-metal. The thickness of all polished pellets were in the range of 450 µm to 480 µm and diameter was 8.7 mm.

## Results and Discussion

X-ray diffraction (XRD) patterns of LATP and LATPBM recorded at room temperature are given in Fig. 1(a). There is no noticeable change found in the XRD peaks of LATP before and after ball milling. The XRD of LATP and LATPBM match with PDF #96-722-2156 having NASICON type structure with rhombohedral unit of space group $R\bar{3}c\ h$. For more structural information and determining crystal lattice parameters, Rietveld refinements are performed on the XRD patterns of LATP and LATPBM powder samples using FullProf Suite. During the refinements, occupancies and thermal parameter were not refined of the atoms. According to refinements results, there is no much difference observed in lattice parameter and cell volume of LATP and LATPBM, as shown in table 1, which confirms that no structural change occurred during ball milling.

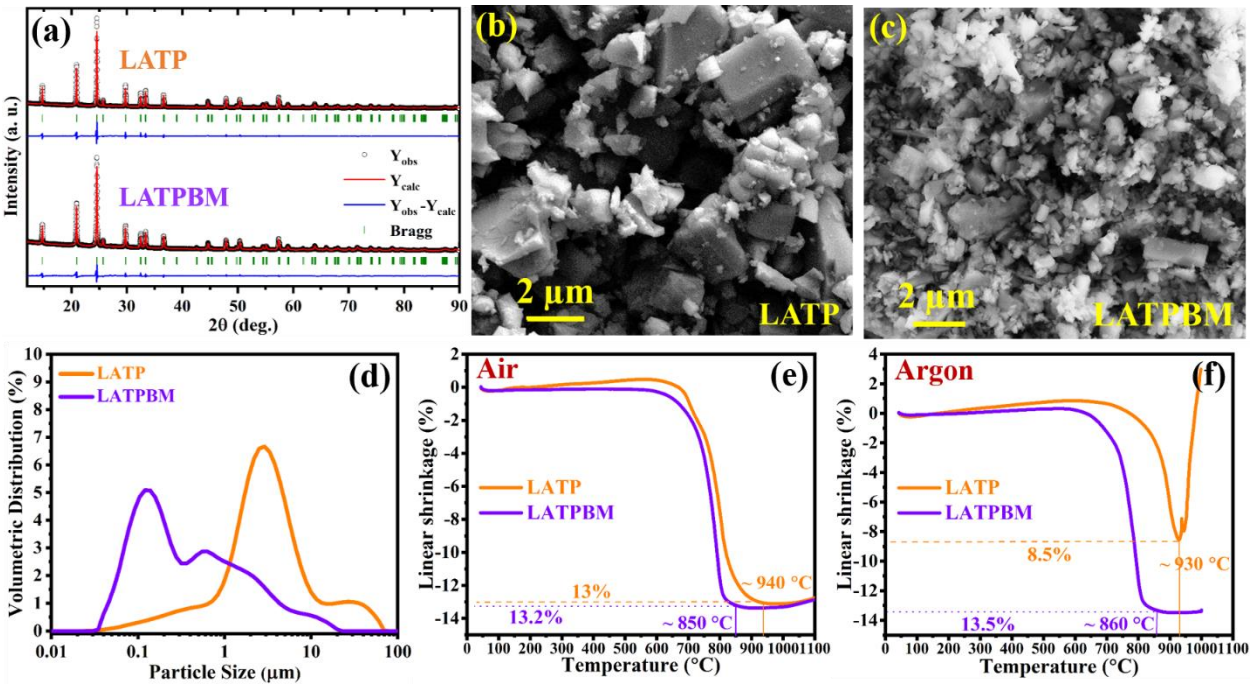


**Figure 1.** Physical measurement of LATP and LATPBM powder samples: (a) Rietveld refinement patterns of LATP and LATPBM powder samples, in the refinement graphs, experimental plot is shown by dotted line (red), calculated by solid line (black), Bragg reflection peaks by vertical lines (green) and difference plot by background line (blue), (b & c) SEM microstructures, (d) granulometry graphs, (e) dilatometry in air, and (f) dilatometry in argon.

The electron microscopic image analysis was done to see the morphological and particle size changes before and after ball milling. From Figs. 1(b & c), it is clearly visible the particles size reduction after ball milling, and morphology that has also changed. The particles size of LATP and LATPBM were further confirmed by granulometry as shown in Fig. 1(d). The average particle size of LATP before ball milling was 3.1 µm which reduced to 0.31 µm after ball milling (LATPBM).

**Table 1.** Lattice parameters determined by Rietveld refinement, and average particle size ($d_{50}$) by granulometry of LATP and LATPBM.

| | a (Å) | b (Å) | c (Å) | V (Å$^3$) | Particle size (µm) |
|---|---|---|---|---|---|
| **LATP** | 8.4944(2) | 8.4944(2) | 20.7783(4) | 1298.405(3) | 3.10 |
| **LATPBM** | 8.4942 (1) | 8.4942 (1) | 20.7780 (6) | 1298.315 (5) | 0.31 |

To determine the sintering temperature and effect of particles size on densification of powder, dilatometry was performed and results are shown in Figs. 1(e & f). Dilatometry graphs recorded in air (Fig. 1e) shows lower sintering temperature of ball milled powder (LATPBM) as compared to LATP before ball milling. The complete densification was observed at 850 °C for LATPBM with 13.2% linear shrinkage as compared to LATP which shows maximum densification at about 940 °C with 13.0% linear shrinkage. The lower particle size with narrow particles distribution not only reduces sintering temperature but also helps achieving higher density [27]. Since, present research is focused on the solutions for full battery fabrication by co-sintering of LATP and phosphate cathode materials. Therefore, sintering behavior of LATP was also observed by dilatometry in argon atmosphere. Similar to air, lower sintering temperature is found for LATPBM in argon also and maximum densification was achieved at about 860 °C with 13.5% linear shrinkage as shown in Fig. 1(f).

However, LATP before ball milling i.e. bigger particles size shows different behavior in argon atmosphere as compared to air. The LATP sample shows densification up to 930 °C temperature and linear shrinkage was reached at 8.5%, but beyond 930 °C temperature, a rapid linear expansion was observed that continued up to a set experimental temperature of 1000 °C. The linear expansion behavior of LATP in argon after 930 °C is required further investigation.

The density of the all sintered pellets was determined by geometric method using formula: $\rho = \frac{m}{V}$ where $m$ is mass of pellet and $V$ is volume of the pellet. The volume of the pellet was calculated

by considering pellet as a cylinder: $V = (A \times h)\ or\ \pi r^2 h$ where, *A*, *r* and *h* are surface area, radius and thickness of the pellets, respectively [23]. The relative density was determined by taking theoretical density of LATP as 2.94 g $cm^{-3}$ and results are shown in tables 2 & 3.

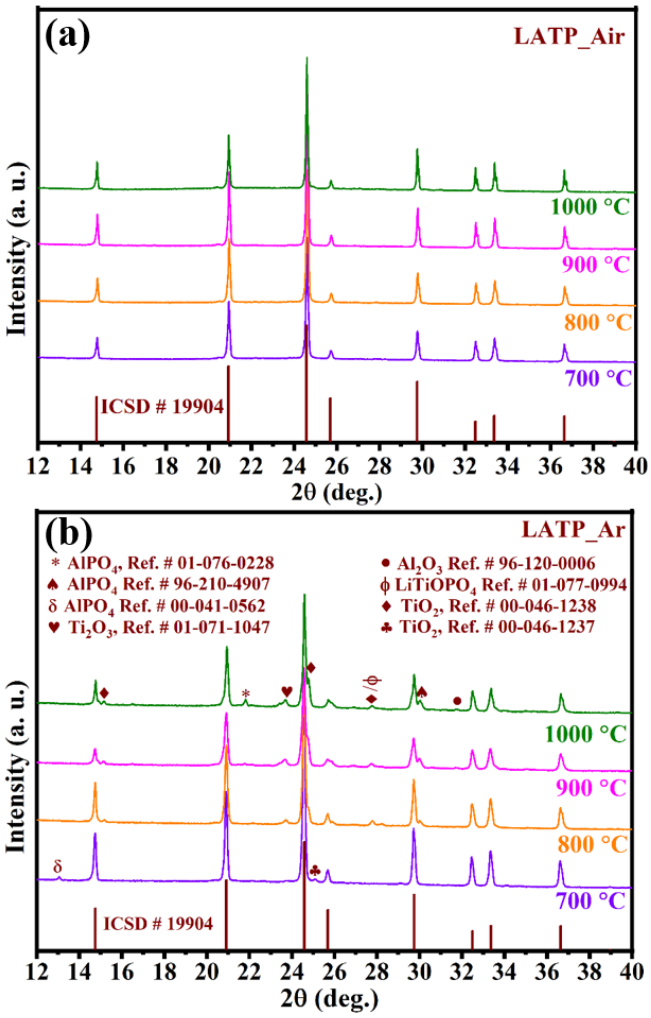


**Figure 2.** XRD data of LATP (before ball milling) pellets sintered at heating rate of 2.5 °C $min^{-1}$ in (a) air, (b) argon.

From the dilatometry results, we have seen that sintering temperatures of LATP before ball milling is higher. Therefore, we have determined the sintering behavior and reactivity of LATP in air and argon at four different temperatures 700 °C, 800 °C, 900 °C, and 1000 °C and heating rate was

kept 2.5 °C $min^{-1}$ for all four samples. XRD data of sintered pellets at different temperatures are shown in Fig. 2. XRD peaks of LATP sintered in air are fully matched with reference patterns of $Li_{1.4}Al_{0.4}Ti_{1.6}(PO_4)_3$ (ICSD # 19904) and no secondary phase was observed up to 1000 °C. The densities of sintered pellets are shown in table 2, and it is found maximum for pellet sintered at 800 °C which decreased with further increasing temperature. The reduction in density with increasing temperature need to be further investigate by microstructure analysis. The density of green pellet was also measured and it was found about 64%. The lattice parameters of LATP pellets samples sintered in air were determined by Rietveld refinement and results are given in supporting information S2.

Contrary to air sintering, LATP shows very differentbehavior when sintered in argon atmosphere. Although, sintering temperatures and heating rate were kept similar as for air sintering. The swelling and cracks were observed in LATP pellets sintered at temperature more than 700 °C. Furthermore, LATP sintered in argon atmosphere shows secondary phases such as $AlPO_4$, $TiO_2$, $LiTiOPO_4$, $Al_2O_2$ and $Ti_2O_3$. These are the common secondary phases which are reported in LATP sintered in air due to Li loss (in the form of $Li_2O$) and decomposition ($AlPO_4$, $TiO_2$ and $LiTiOPO_4$) [11, 26-28] except $Ti_2O_3$ phase. The secondary phase $Ti_2O_3$ ($Ti^{3+}$) can be expected only if reduction of Ti ($Ti^{4+} \rightarrow Ti^{3+}$) occurs in argon atmosphere, this is also the reason of color change of pellets [29]. However, some of the secondary phases are reported beneficial for sintering process such as $AlPO_4$ helps in removing voids/pores and increases density of LATP [22, 24]. Similarly, optimum content of $LiTiOPO_4$ helps in decreasing sintering temperature and enhances densification [24]. The excess content of these phases hinders Li-ion diffusion at grain boundary due to low conductivity of these phases [24, 27, 28]. The phase quantification of LATP using Rietveld

refinement could not have achieved successfully due to multiphase compositions of samples and common peaks position of multiple phases.

**Table 2.** Relative density, activation energy, conductivity at 25 °C of LATP pellets sintered in air (left) and argon (right).

| | **LATP_Air** | | | **LATP_Ar** | | |
|---|---|---|---|---|---|---|
| **Temp.** | **Relative density (%)** | **Total conductivity (S cm$^{-1}$)** | **Activation energy $E_a$ (eV)** | **Relative density (%)** | **Total conductivity (S cm$^{-1}$)** | **Activation energy $E_a$ (eV)** |
| **700 °C** | 76.7 | $3.43\times10^{-5}$ | 0.39 | 75.0 | $4.69\times10^{-5}$ | 0.40 |
| **800 °C** | 94.8 | $1.93\times10^{-4}$ | 0.36 | 89.3 | $3.28\times10^{-5}$ | 0.35 |
| **900 °C** | 92.5 | $1.04\times10^{-4}$ | 0.37 | 74.5 | $2.76\times10^{-5}$ | 0.40 |
| **1000 °C** | 89.1 | $4.02\times10^{-5}$ | 0.37 | 65.8 | $6.02\times10^{-5}$ | 0.27 |

SEM microstructures of LATP pellets sintered in air are shown in Figs. 3(a-d). The pellet sintered at 700 °C shows isolated particles of LATP suggesting insufficient temperature for sintering, which can also infer to lowest density of 76.7% shown in table 2. The microstructure of pellet sintered at 800 °C shows inter-connected grains contributing to high density 94.8% of the sample. In the microstructure of pellet sintered at 900 °C, bigger grains can be seen formed by inter-diffusion of small particles as shown in magnified view (inset of Fig. 3c). The grain growth continues for sample sintered at 1000 °C and small grains completely diffused to bigger grains [23, 26]. However, reduction in density is observed for the pellets sintered at 900 °C and 1000 °C,

which could be due to an inhomogeneous grain growth leading to grain boundary de-cohesion of the bigger grains. The separation of grains and microcracks formation are clearly visible in magnified view of sample sintered 1000 °C. The lower density due to lack of cohesion among bigger grains was also observed in the previous studies [11, 26, 27].

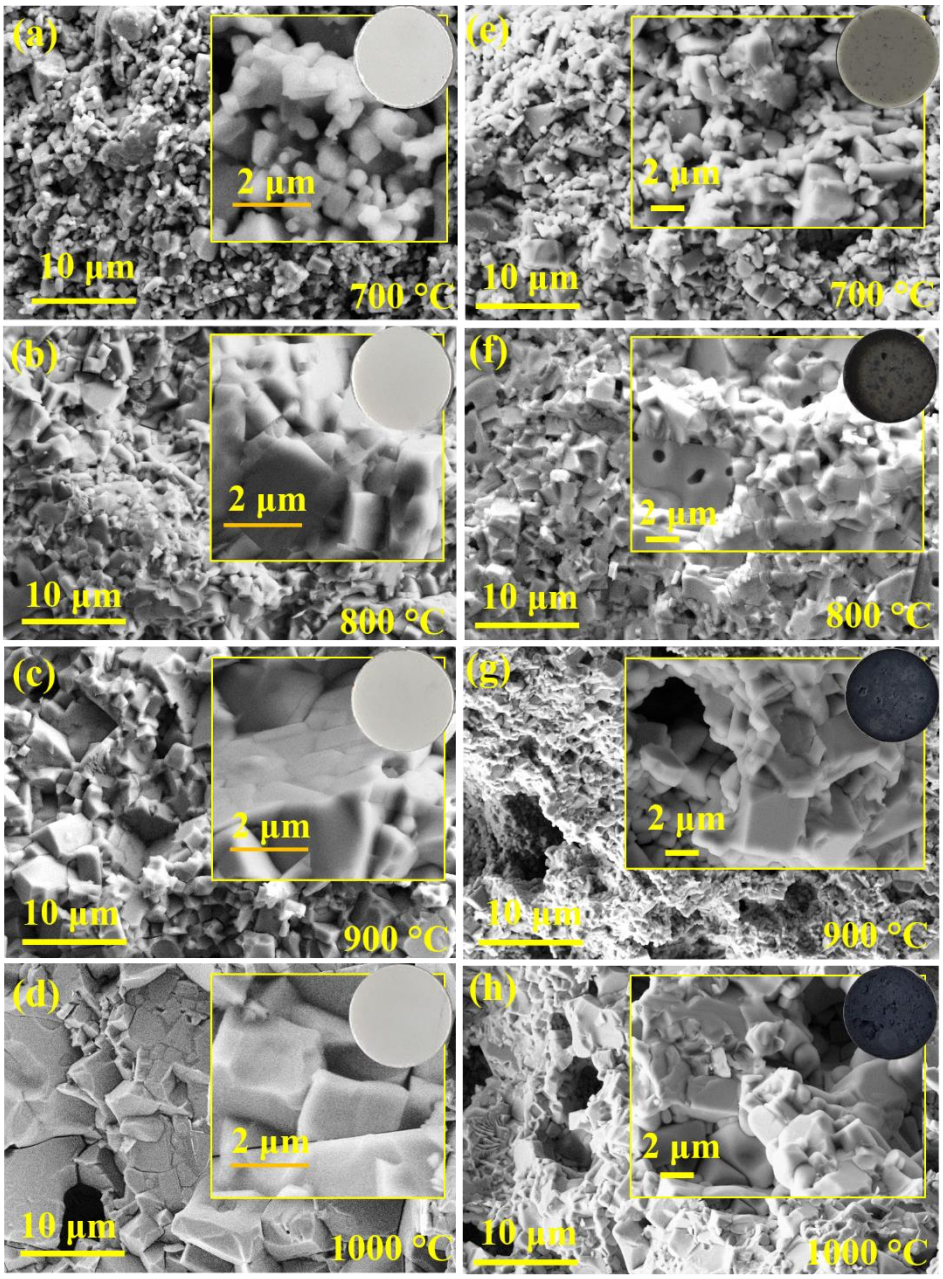

**Figure 3.** SEM images of LATP pellets (cross section) sintered in (a-d) air, (e-h) argon; magnified view of microstructures and photographs of pellets are given in inset of respected image.

SEM images shown in Figs. 3(e-h) illustrates that microstructure of LATP are highly effected by sintering in argon atmosphere. The swelling and micro cracks/pores were observed in LATP pellets sintered at higher than 700 °C, and even color of pellets was also changed from white to blue (inset photographs of pellets). The size of pores increases from 800 °C to 1000 °C, and pellets sintered at 900 °C and 1000 °C become almost porous. Although, changes in the pellets are started at 700 °C which can be seen by grey color with dark spots in photograph of pellets (inset of Fig. 3e). These changes were further grown with increasing temperature.

The microstructure analysis of LATP sintered in argon can be co-related to previous results. The swelling/pores phenomenon of pellets could relate to dilatometry results of LATP in argon which shows linear expansion after 930°C (Fig. 1f). The porous structure and larger size of microcracks can be co-related to the very low density (table 2) of pellets sintered in argon. The color change of pellets can relate to Ti reduction which is further confirmed by $Ti_2O_3$ phase found in XRD patterns (Fig. 2(b)). The color change of sintered LATP pellets in reductive $Ar/H_2$ atmosphere was reported previously [29]. However, Ar atmosphere seems sufficient to reduce LATP at high temperature, as reported for $TiO_2$ phase [30]. In addition, some of the reasons of micro crack/pores formation in the pellets could be related to the literature [24, 27, 28, 31-33]; (i) the dark grey spots in the pellets could be due to agglomeration of $AlPO_4$ phase which is also considered possible reason for other secondary phases like $TiO_2$ and $LiTiOPO_4$ [24, 27], (ii) pores might be created on removal of Li in the form of $Li_2O$ due to decomposition of LATP ($LATP \rightarrow AlPO_4 + TiO_2 + Li_2O_g$) [27], (iii) larger particles size i.e. 3.1 µm (higher than critical size of 2 µm considered for $LiTi_2PO_4$ type materials) of LATP leading to higher anisotropic thermal expansion effect [31-33], and beyond

the critical size, microcracking is expected in the coarser grains. These microcracks also contributes to the lower conductivity of LATP pellets [28].

To analyze the impact of secondary phases, microcracks and density on conductivity of sintered pellets, AC impedance spectroscopy study was performed on samples sintered in air and argon. Fig. 4 shows the impedance diagrams measured at -20 °C for two sample of LATP sintered under air, i.e. 800 °C (Fig. 4a) and 1000 °C (Fig. 4.b). The shape of the impedance diagrams of the samples was similar and it consisted of only one depressed semi-circle slightly offset from the origin. Using the equivalent circuit described in Fig. 4, we determined the resistance $R_1$ of the grain and the resistance $R_2$ and the capacitance $C_2$ associated with the semicircle. The calculated capacitance for the semicircle is equal to $2.0\times10^{-9}$ F ($R_2C_2\omega°=1$) for the two samples. This value corresponds to the electrical response associated with the blocking phenomenon related to microstructural defects such as grain boundaries, pores, and cracks. In fact, in solid ionic conductors, the microstructural defects (supposed to be pores, grain boundaries, cracks or insulating inclusions) lead to an internal blocking phenomenon of a fraction of mobile charge carriers [34]. This phenomenon is described as a blocking process at the internal interface and leads to a decrease in the electrical conductivity of the material.

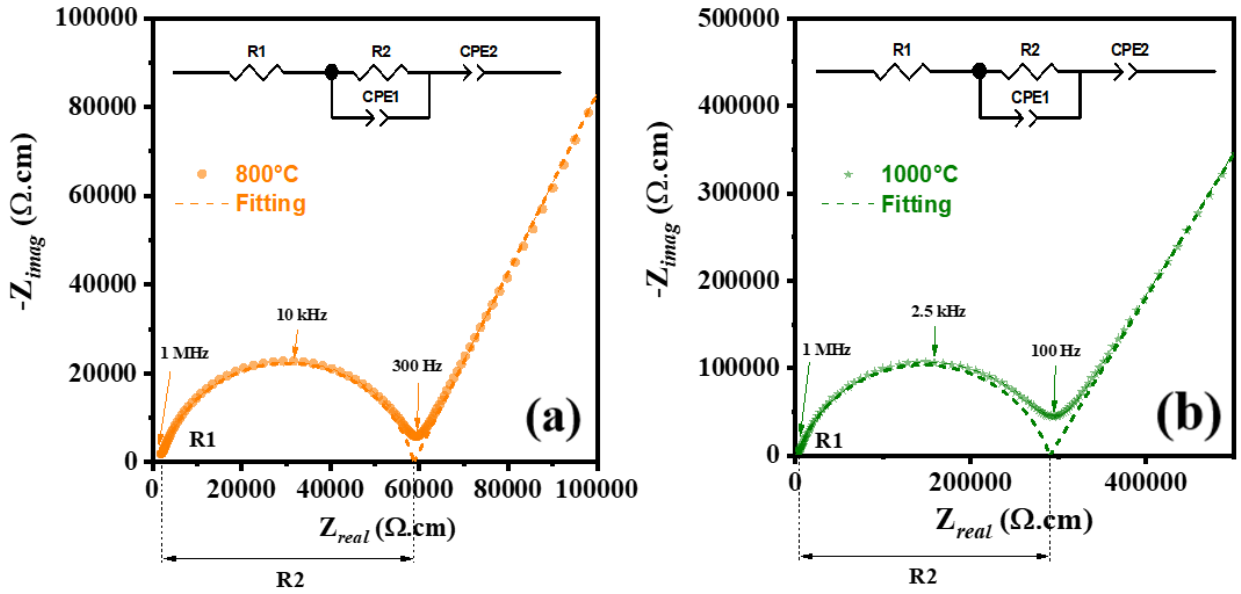


**Figure 4.** Impedance diagrams measured at -20 °C with fitting of (a) LATP-Air 800°C, and (b) LATP-Air 1000 °C.

In doing so, a direct and simple link can be made between the increase in the semi-circle, corresponding to the increase in blocking between grains, and the deterioration of the grain boundaries as the sintering temperature increases (see the micrographs Fig. 3) [35]. The intrinsic conductivity of the material can be calculated from the grain resistance ($R_1$) but the semicircle amplitude is very large compared to $R_1$ which leads to a significant uncertainty in the determination of $R_1$. In this case, we determined only the total conductivity of the samples from the total resistance of the sample given by ($R_1 + R_2$).

Figs. 5(a & c) compiles the Nyquist plots of LATP pellets measured at 25 °C for all sintered samples, whereas activation energies calculated from linear extrapolation of the Arrhenius plot are shown in Figs. 5(b & d). The conductivities obtained at 25 °C and activation energies of all LATP samples are shown in table 2. The conductivity of the pellets sintered in air are directly in correlation with density of pellets. The maximum conductivity of $1.93\times10^{-4}$ S $cm^{-1}$ at 25 °C was

recorded for the samples sintered at 800 °C in air. The similar sample also shows lowest activation energy ($E_a$ = 0.36 eV) in its group. However, reduction in conductivity was noticed when temperature increases to 900 °C and 1000 °C. This could be due to the separation of coarser grains as observed in SEM images, resulting in lower density for these samples. The samples having higher density (and less microstructural defects) show higher conductivity due to easy paths for Li-ion migration, this behavior being broadly reported in literature [23, 26, 27].

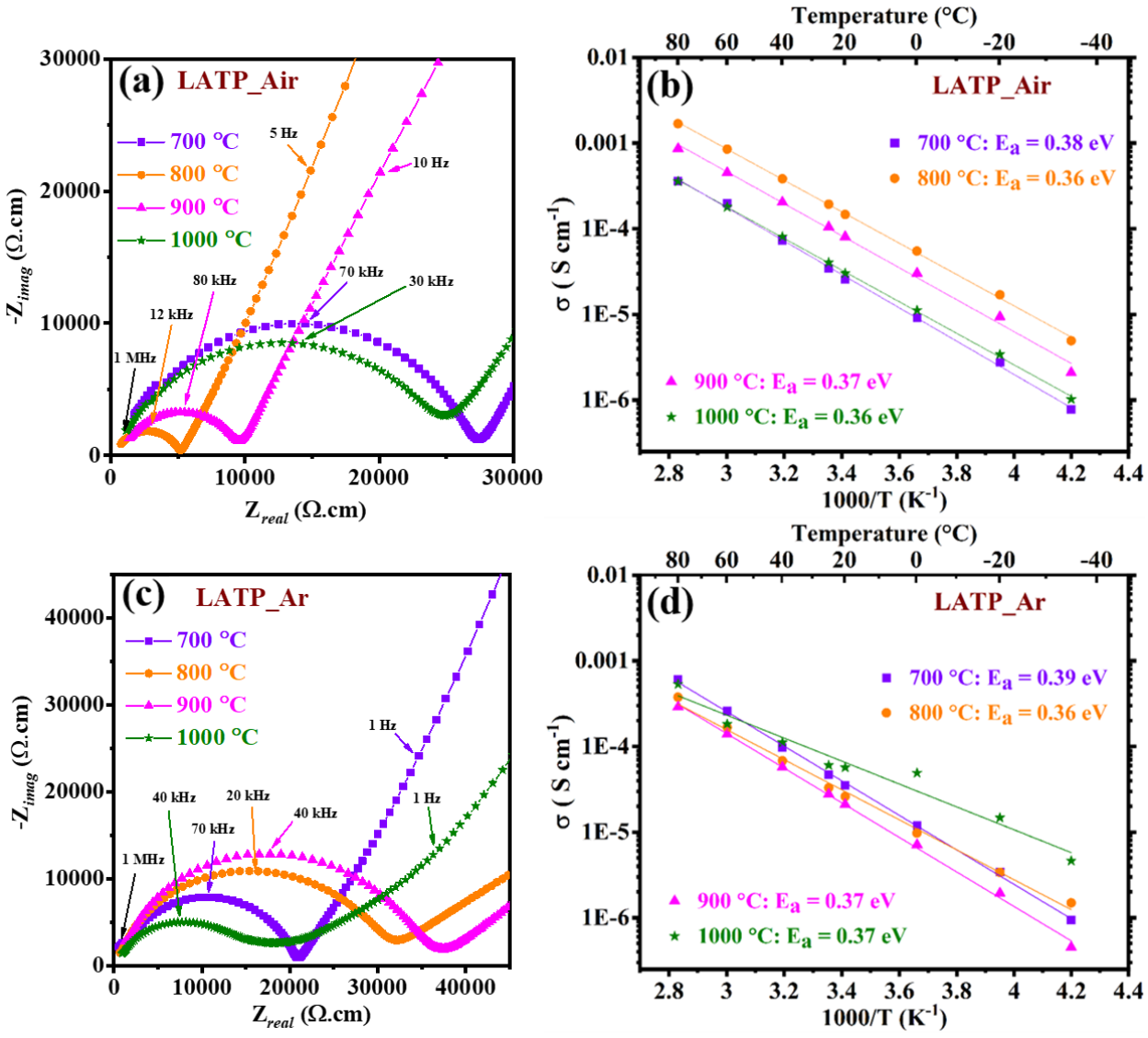

**Figure 5.** Nyquist plots recorded at 25 °C and Arrhenius plots of LATP pellets sintered in (a, b) air, (c, d) argon.

The samples sintered in argon show lower conductivities and higher activation energies as compared to samples sintered in air. The low conductivity can be directly related to secondary phases, microstructure, and density of LATP pellets sintered in argon. The secondary phases $AlPO_4$ and $LiTiOPO_4$ agglomerate at grain boundaries, blocking the Li-ion transport [24]. As previously described, the microcracks and pores present in the pellets also hinder the grain boundary connectivity, leading to blockage in ion transport [26, 27]. However, pellet sintered at 700 °C shows higher conductivity despite of lower density which is contrary to sample sintered at 800 °C. This can be related to higher number of secondary phases and pores present in the sample sintered at 800 °C leading to lower conductivity. The conductivity further decreases for sample sintered at 900 °C due to bigger size of microcracks causing lower density. However, in spite of large size of microcracks, lower density and high intensity peaks of secondary phases, the sample sintered at 1000 °C shows higher conductivity and lower activation energy. The reason of strange results at 1000 °C is not fully understood. Furthermore, it can be inferred to contribution of Pt in lower resistance due to highly porous pellet. During Pt sputtering on highly porous pellet, Pt can enter inside the pores of pellet providing a conducting path for electrons. However, these are the possibilities, exact reason is still not clear.

In conclusion, till now, we have observed the overall issues with LATP sintered in argon atmosphere: (i) microcracking and pores, (ii) secondary phases ($AlPO_4$, $LiTiOPO_4$, $TiO_2$ and $Ti_2O_3$) (iii) Li evaporation in the form of $Li_2O$ and (iv) reduction of Ti ($Ti^{4+} \rightarrow Ti^{3+}$). Therefore, further study will focus on solving these issues with LATP in argon atmosphere.

To avoid the microcracking and bring down the particle size in the range of critical size of LATP (< 2 µm), ball milling was done on LATP as described above. On the basis of dilatometry results of LATPBM as shown in Figs. 1(e & f), we have restricted the sintering temperature range and selected three sintering temperatures 800 °C, 850 °C and 900 °C. However, heating rate was kept 2.5 °C $min^{-1}$, similarly to LATP samples before ball milling. Furthermore, to compensate the Li loss from the sample during sintering, LATPBM pellets were covered with bare LATP powder.

XRD data of LATPBM samples sintered in argon at heating rate of 2.5 °C $min^{-1}$ is shown in Fig. 6 (a). It can be seen from the XRD patterns that all three samples sintered at 800 °C, 850 °C and 900 °C are still showing secondary phases of $LiTiOPO_4$, $AlPO_4$ and $Ti_2O_3$. However, secondary phase $TiO_2$ disappeared from all three samples which forms, generally, due to Li loss ($LATP \rightarrow AlPO_4 + TiO_2 + Li_2O_g$) [27]. Therefore, it can be concluded that Li loss is avoided by covering the pellet with bare powder. Furthermore, microcracking and pores are not visible in the pellets of LATPBM prepared by lower particles size as shown in SEM images and photographs of pellets (supporting information Fig. S3). Therefore, particle size lower than critical size plays an important role to avoid cracks in LATP, which was reported previously [28]. The secondary phase $Ti_2O_3$ is still present due to reduction of Ti (color of pellet was also changed from white to blue). Based on the XRD results shown in Fig. 6(a), it can be concluded that, we have overcome the issues of cracks/pores and Li loss during sintering by reducing particle size and pellets covering, respectively. Although, other secondary phases $Ti_2O_3$ due to Ti reduction, and $LiTiOPO_4$ and $AlPO_4$ due to decomposition of LATP are still present in the LATPBM samples sintered in argon at heating rate of 2.5 °C $min^{-1}$.

Therefore, we have further changed the sintering parameters to find the exact cause of secondary phase formation. When heating rate was reduced from 2.5 °C $min^{-1}$ to 1.5 °C $min^{-1}$, high purity

XRD data without having cracks and any secondary phase was found for the sample sintered at 800 °C in argon atmosphere, and grains de-cohesion was found at 850 °C and 900 °C. The heating rate was further reduced to 1.0 °C $min^{-1}$, again found pure phase of LATPBM without having any secondary phases or cracks/pores at 800 °C as shown in Fig. 6(b). Therefore, it can be concluded that for sintering LATP in argon atmosphere, heating rate should be equal or less than 1.5 °C $min^{-1}$ to avoid any secondary phase and cracks. This phenomenon can be related to homogeneous heating i.e. a sufficient lower heating rate is required to dissipate the heat homogeneously inside the pellet for uniform densification. In the absence of homogeneous heating, part of sample may convert into other secondary phases and also may cause partial reduction of Ti in inert atmosphere.

For the comparative study, LATPBM samples also sintered in air and XRD patterns are shown in Fig. 6(c). The XRD peaks of LATPBM sintered in air are fully matched with reference patterns of $Li_{1.4}Al_{0.4}Ti_{1.6}(PO_4)_3$ (ICSD # 19904) and no secondary phase was observed at all three temperatures 800 °C, 850 °C and 900 °C. Therefore, sintering of LATP and LATPBM in air does not impact the phase purity. Although, heating rate shows great impact on phase purity of LATP and LATPBM under argon gas sintering. However, it is not fully clear that why inhomogeneous heating effect was seen in argon atmosphere only. The Rietveld refinement was performed to determine the lattice parameters of LATPBM sintered in argon (1.0 °C $min^{-1}$) and air (2.5 °C $min^{-1}$), and results are given in supporting information S4 & S5, respectively.

The micrographs and photographs (inset) of LATPBM pellets sintered in argon and air are shown in Figs. 6(d-i), and relative density is shown in table 3. The LATPBM pellets sintered at 800 °C show maximum densities of 98.1% and 97.8% in both argon and air, respectively which decrease with further increasing the temperature at 850 °C and 900 °C. The behavior of density reduction at higher temperature is also observed for pellets of non-ball milled LATP. This behavior can be

correlated to SEM images of the respective pellets. The pellets sintered at 800 °C show fully dense microstructure with almost homogenous grain size. When the temperature increases to 850 °C, some of the grains have grown much bigger in size as compared to other grains creating inhomogeneity. Moreover, in the microstructure of pellets sintered at 900 °C, majority of grains having bigger size show grain boundary de-cohesion. Furthermore, we can see the slight yellowish color of LATPBM pellets sintered in Ar (inset of Figs. 6d-6f). There may be several possibilities of color change of LATPBM pellets during Ar sintering. The color change could be possible due to change in microstructures. During the sintering, grain boundaries are formed and the porosity is reduced, therefore, absorption and scattering of the light by the sample also change. The color change could also possible due to change in oxygen vacancies which leads to very early stage of surface reduction, however, the reduction is too small to quantify by XRD.

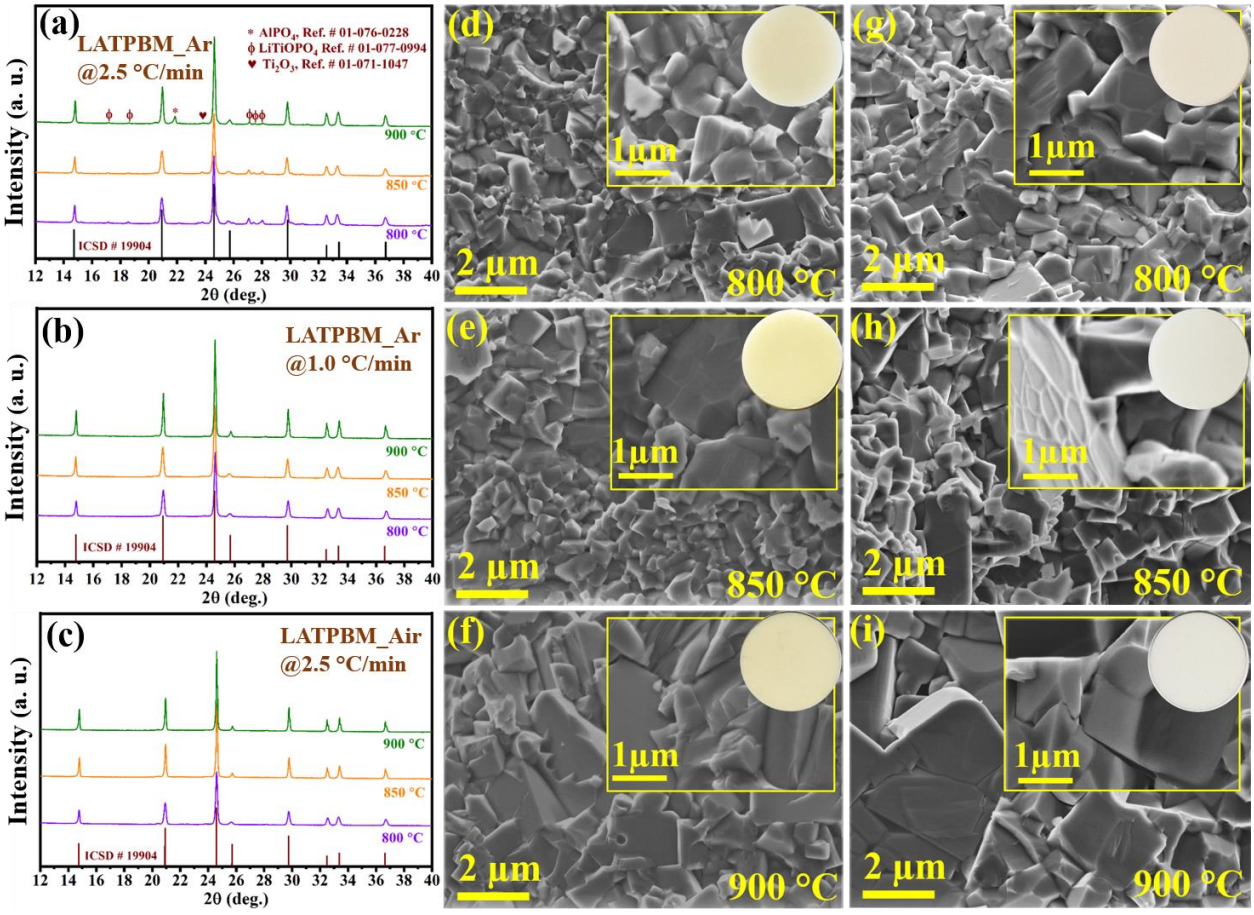


**Figure 6.** (a, b) XRD of LATPBM pellets sintered in argon atmosphere at heating rate of (a) 2.5 °C $min^{-1}$ (b) 1.0 °C $min^{-1}$, (c) LATPBM pellets sintered in air at heating rate of 2.5 °C $min^{-1}$, and (d-f) SEM images LATPBM pellets sintered in argon at heating rate of 1.0 °C $min^{-1}$, and (g-i) SEM images LATPBM pellets sintered in air at heating rate of 2.5 °C $min^{-1}$.

To determine the impact of homogeneous/inhomogeneous grain growth on the conductivity of LATPBM pellets, AC impedance spectroscopy study was performed using the similar conditions as for non-ball milled LATP and the results are shown in Fig. 7.

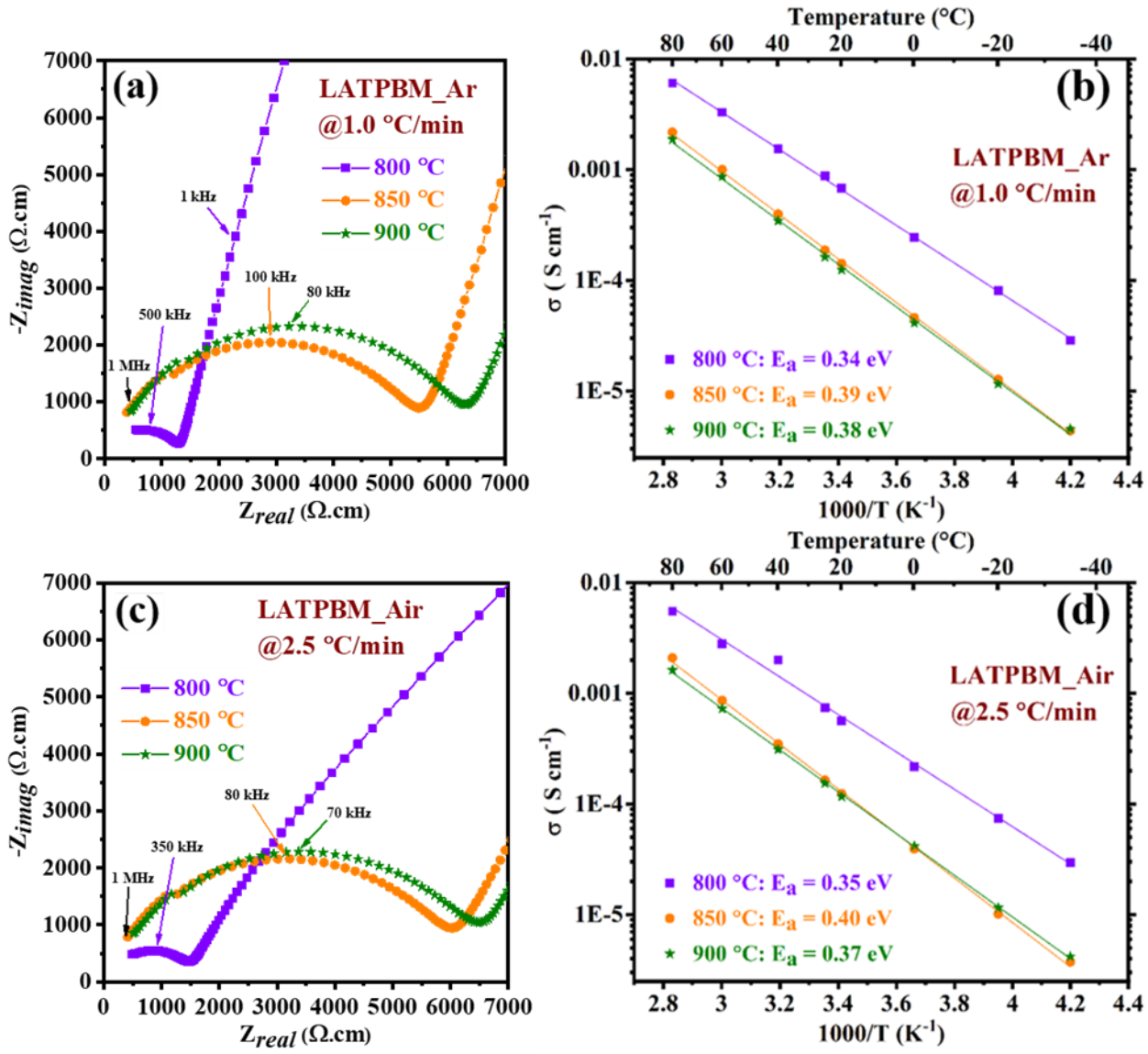


**Figure 7.** Nyquist plots recorded at 25 °C and Arrhenius plots of LATPBM pellets sintered in (a, b) argon at heating rate of 1.0°C $min^{-1}$ and (c, d) air at heating rate of 2.5 °C $min^{-1}$.

The impedance results show direct correlation of density and microstructure with conductivity of the pellets sintered in both types of environments argon and air. Comparison of the diagram at -20 °C for LATPBM samples sintered under argon at 800 °C and 900 °C with heating rate of 1.0 °C $min^{-1}$ can be found in supporting information (Fig. S6), showing the similar behavior that was before ball-milling. The maximum conductivity $8.77\times10^{-4}$ S $cm^{-1}$ at 25 °C was recorded for the

sample sintered at 800 °C in argon, which is very close to the highest conductivity $1.0\times10^{-3}$ S $cm^{-1}$ at room temperature reported for LATP [36]. This sample also shows maximum relative density of 98.1%. Similarly, the pellet sintered in air at 800 °C also shows highest conductivity of $6.66\times10^{-4}$ S $cm^{-1}$ at 25 °C in its group. These similar pellets also show lowest activation energy in their groups as shown in table 3. Pellets sintered at 800 °C show 4-5 times higher conductivity as compared to conductivities of pellets sintered at 850 °C in both argon and air. This relate to the microstructure of the pellets. The pellets sintered at 800 °C show more homogeneous grain growth as compared to 850 °C, which can provide easy and short path to Li-ions diffusion [33]. Whereas, inhomogeneous grain size can affect the diffusion of Li-ions at the grain boundary of bigger and smaller grains due to mismatching of the grain boundaries and microstructural defects leading to decrease in both conductivity and relative density. The separation/de-cohesion in the grain boundaries of bigger grains of pellets sintered at 900 °C are the main cause of lower conductivity. The EIS date of LATPBM pellets sintered in argon at heating rate of 2.5 °C $min^{-1}$ is given in supporting information S7 & S8.

From the microstructure and impedance results, one could conclude that once the pellets achieve maximum density irrespective of temperature, sintering temperature should not be increased. Beyond the optimum temperature, samples show difficulties in Li-ions diffusion which leads to lower conductivities. In our study performed on LATPBM samples, we have achieved 98.1% density and highest conductivity at relatively low temperature of 800 °C in argon atmosphere. These results would be very helpful for solid state battery fabrication by co-sintering process because 800 °C is an acceptable temperature for cathode materials such as $LiFePO_4$ [29] and $Li_3V_2(PO_4)_3$.

**Table 3.** Relative density, activation energy, conductivity at 25 °C of LATPBM pellets sintered in argon at heating rate of 1.0 °C $min^{-1}$ (left) and in air at 2.5 °C $min^{-1}$ (right).

| | **LATPBM_Ar** | | | **LATPBM_Air** | | |
|---|---|---|---|---|---|---|
| **Temp.** | **Relative density (%)** | **Total conductivity (S $cm^{-1}$)** | **Activation energy $E_a$ (eV)** | **Relative density (%)** | **Total conductivity (S $cm^{-1}$)** | **Activation energy $E_a$ (eV)** |
| **800 °C** | 98.1 | $8.77\times10^{-4}$ | 0.34 | 97.8 | $6.66\times10^{-4}$ | 0.35 |
| **850 °C** | 97.0 | $1.86\times10^{-4}$ | 0.40 | 95.4 | $1.64\times10^{-4}$ | 0.40 |
| **900 °C** | 93.7 | $1.62\times10^{-4}$ | 0.38 | 95.0 | $1.53\times10^{-4}$ | 0.37 |

Furthermore, we have also recorded electrochemical performances of LATP and LATPBM samples sintered at 800 °C in air and argon with Li-metal in symmetric cell (Li/LATPBM/Li) at current densities of 0.005, 0.01 and 0.05 mA $cm^{-2}$ and results are shown in Fig. 8. Moreover, it is well known that LATP is unstable with Li-metal due to dendrite formation and Ti reduction [37, 38]. To stabilize the interface of LATP and Li-metal, an additional layer of $Al_2O_3$ [37], $Li_3PO_4$ [37, 39], PEO [40, 41] between LATP and Li-metal has been studied with improved results. The interfacial resistance and stability may depend on many factors such as thickness of LATP pellet, proper contact between SE and Li-metal, thickness of Li-metal, density of LATP pellet and type of additional layer between LATP and Li-metal etc. We have not optimized these factors in the current work, for that, a separate study has been done and will be published in future. However, a clear difference in the resistances of LATP and LATPBM pellets can be seen. The LATPBM pellets show a great improvement in the resistance as well as stability with Li metal because of

high density and pure phase. In addition, LATP pellet sintered at 800°C in Ar atmosphere shows very poor performance compared to the one sintered in air. The LATP in Ar is quite reduced, lower density and many impurity phases in the sample, whereas, LATP sintered in air at 800°C is quite dense and pure phase. Furthermore, our samples have shown lower interfacial resistance and better stability against Li-metal as compared to previous studies done for bare LATP [37, 39, 42].

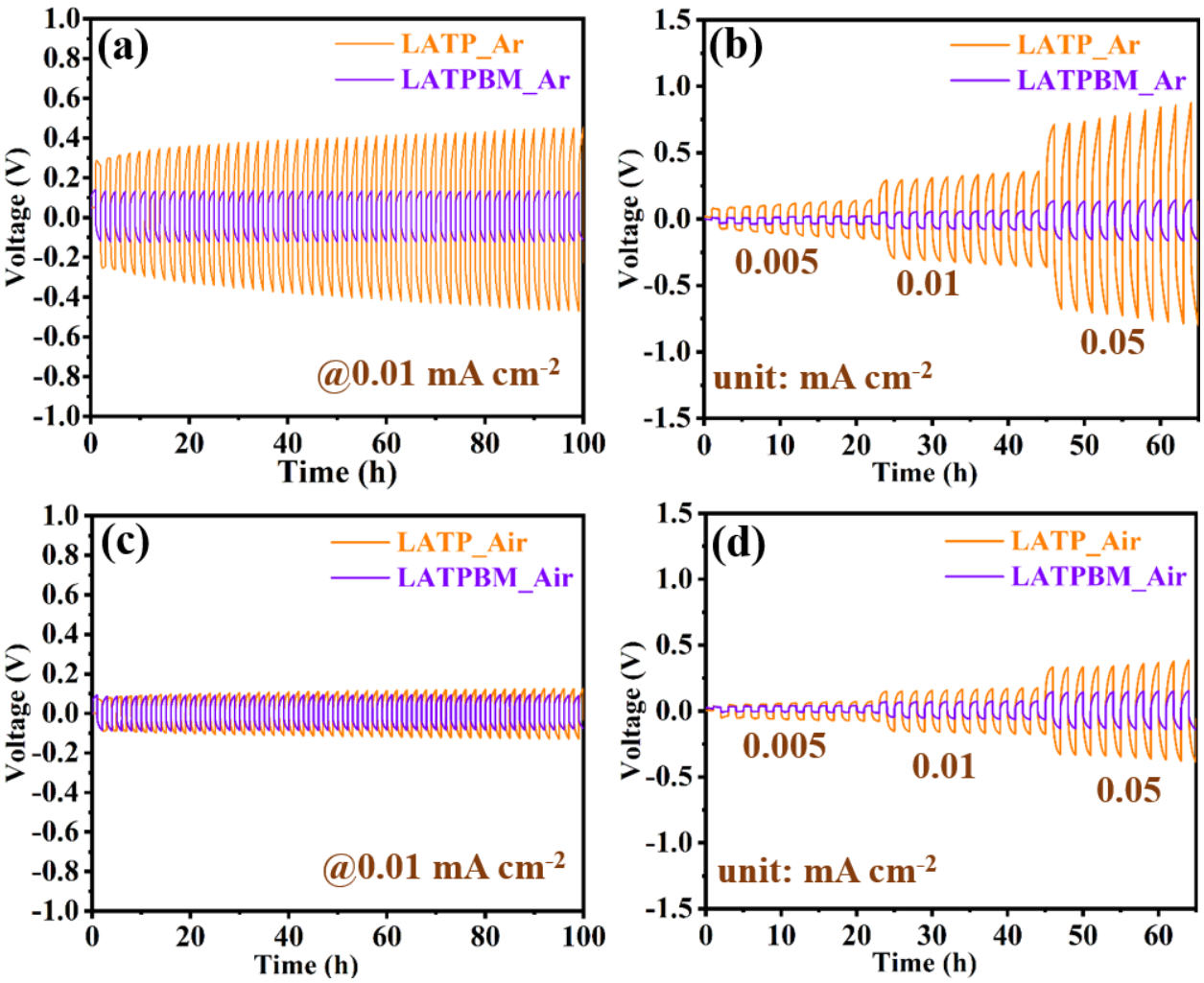


**Figure 8.** Electrochemical behavior of the symmetrical cells at current densities of 0.005, 0.01 and 0.05 mA $cm^{-2}$ of (a, b) LATP and LATPBM sintered in argon at 800 °C, (c, d) LATP and LATPBM sintered in air at 800 °C.

At the end, we have also studied the anisotropic thermal expansion behavior of LATP by thermodiffraction in $N_2$ atmosphere (incompatibility of argon gas to instrument) as shown in Fig. 9. The first XRD pattern was collected at 30 °C, then temperature raised to 600 °C as sintering temperature in our study was also more than 600 °C. From 600 °C to 950 °C, XRD data was collected after every 50 °C during heating and every 100 °C during cooling. The XRD patterns show continuous shifting of peaks with increasing temperature which came back to original positions during cooling as show in Figs. 9(a & b). From the peak position analysis, we can say that thermal expansion in LATP is reversible.

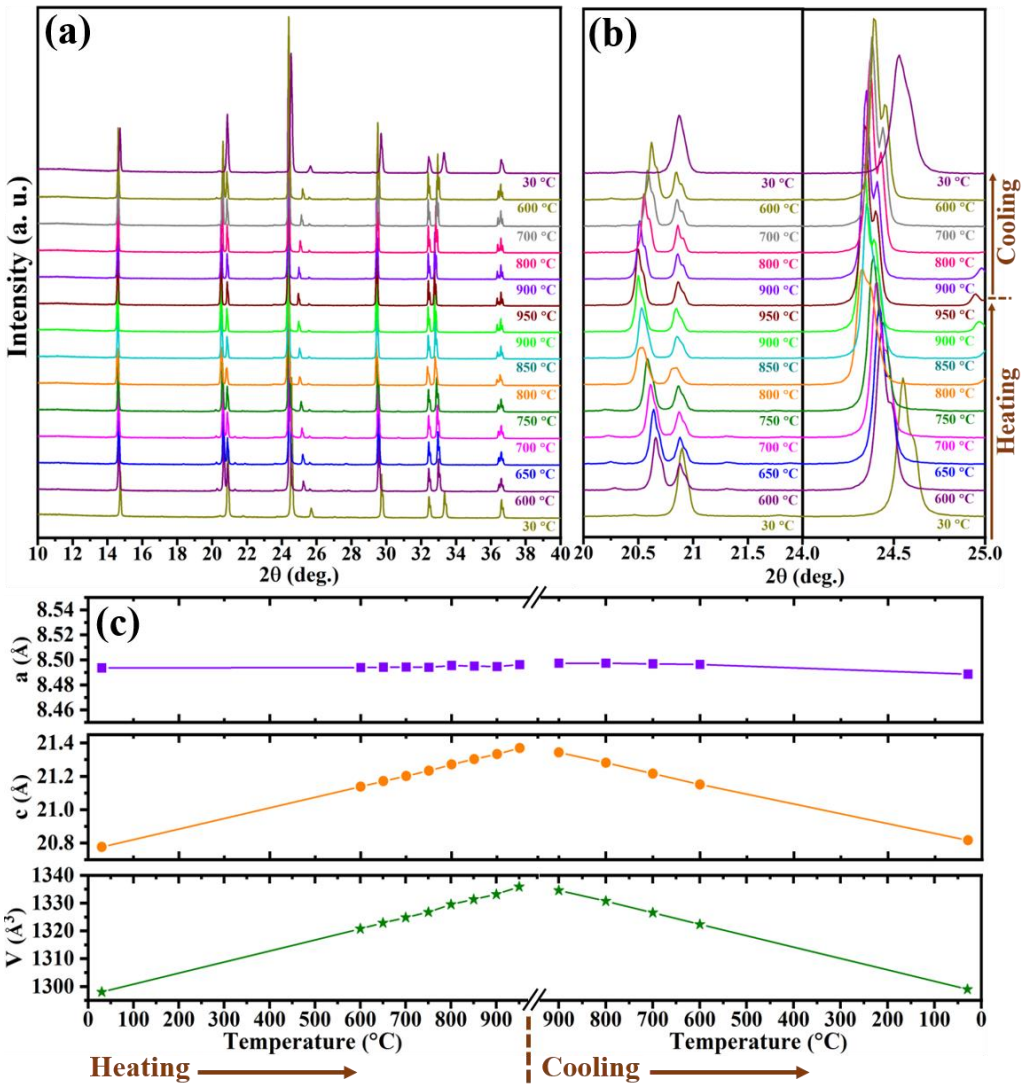

**Figure 9.** (a) Thermodiffraction of LATP under inert $N_2$ atmosphere, (b) magnified view for showing peak shifting, (c) variation in cell parameters and volume of LATP unit cell with temperature during heating and cooling determined by Rietveld refinement.

For more details, Rietveld refinement was performed on the all XRD patterns to determine the change in lattice parameters and volume of the LATP unit cell with temperature during heating and cooling and results are plotted in Fig. 9(c). The values of lattice parameters are given in table S9 of supporting information. The results show that lattice parameter *a* varies little bit, whereas, a large variation in lattice parameter *c* and cell volume *V* is noticed from 30 °C to 950 °C. This anisotropic thermal expansion in lattice parameters *a* and *c* is considered one of the reasons for microcracking in LATP pellets during sintering [31-33]. Furthermore, impact of anisotropic thermal expansion is found more on bigger particle size of LATP (higher than critical size) in pellets as compared to lower size of particles. However, anisotropic thermal expansion is a material specific behavior but present study shows that its effect on applications of LATP can be reduced by optimizing the physical properties and sintering condition of LATP material.

## Conclusion

The present work focuses on the sintering behavior of $Li_{1.4}Al_{0.4}Ti_{1.6}(PO_4)_3$ (LATP) solid electrolyte in argon atmosphere as a function of particle size and sintering conditions. The LATP pellets prepared with powder of bigger particles size (3.1 µm) show many secondary phases and cracks/pores in the pellets during sintering in argon atmosphere. Whereas, no such issue was found for the pellets sintered in air. Therefore, to stabilize the LATP in argon atmosphere, particle size of powder was reduced to 0.31 µm by ball milling. The pellets of ball milled LATP (LATPBM) does not only solve the issue of cracks/pores issue but also decreased the sintering temperature as confirmed by dilatometry. However, secondary phases were eliminated from the LATPBM samples by decreasing the heating rate from 2.5 °C $min^{-1}$ to 1.0 °C $min^{-1}$ during sintering in argon atmosphere. The smaller particle size and slow heating rate have provided uniform densification without any impurity phase, and density has reached more than 98%. Furthermore, we have not only stabilized the LATP in argon atmosphere but also achieved the high conductivity of $8.77\times10^{-4}$ S $cm^{-1}$ at 25 °C for the pellet sintered at just 800 °C. Therefore, the present research work can play an important role in solid state battery fabrication by co-sintering process with state of art cathodes such as $LiFePO_4$ and $Li_3V_2(PO_4)_3$.

"**Supporting Information:** Additional results including graphs, microstructure and analysis data"

## Acknowledgements

The authors thank S. Duffourt, S. Gascoin, H. Laurence, X. Larose and J. Lecourt for technical help. We gratefully acknowledge the CNRS, the Minister of Education and Research, Normandy region and the ANR through the project Flashbat contract no. ANR-20-CE05-0040-02. The authors Hari Raj and Valerie Pralong also acknowledge funding from the European Union's Horizon 2020 research and innovation programme under the Marie Skłodowska Curie grant agreement No. 101034329 and WINNINGNormandy Program supported by the Normandy Region.

## References


1. Janek, J.; Zeier, W.G. A solid future for battery development. *Nat. Energy* **2016,** *1*, 16141.

2. Xu, L.; Tang, S.; Cheng, Y.; Wang, K.; Liang, J.; Liu, C.; Cao, Y. C.; Wei, F.; Mai, L. Interfaces in Solid-State Lithium Batteries. *Joule* **2018,** *2,* 1991–2015.

3. Armand, M.; Tarascon, J. M. Building better batteries. *Nature* **2008,** *451,* 652–657.

4. Tarascon, J. M.; Armand, M. Issues and challenges facing rechargeable lithium batteries. *Nature* **2001,** *414,* 359–367.

5. Li, M. X.; Wang, X. W.; Wang, Y. F.; Chen, B. W.; Wu, Y. P.; Holze, R. A gel polymer electrolyte based on composite of nonwoven fabric and methyl cellulose with good performance for lithium ion batteries. *RSC Adv.* **2015,** *5,* 52382–52387.

6. Scrosati, B.; Garche, J. Lithium batteries: Status, prospects and future. *J. Power Sources* 2**010,** *195,* 2419–2430.

7. Manthiram, A.; Yu, X. W.; Wang, S. F. Lithium battery chemistries enabled by solid-state electrolytes. *Nat. Rev. Mater.* **2017,** *2,* 16103.

8. Ren, Y.; Chen, K.; Chen, R.; Liu, T.; Zhang, Y.; Nan, C. W. Oxide Electrolytes for Lithium Batteries. *J. Am. Ceram. Soc.* **2015,** *98 (12),* 3603–3623.

9. Zheng, Y.; Yao, Y.; Ou, J.; Li, M.; Luo, D.; Dou, H.; Li, Z.; Amine, K.; Yu, A.; Chen, Z. A review of composite solid-state electrolytes for lithium batteries: fundamentals, key materials and advanced structures. *Chem. Soc. Rev.* **2020,** *49,* 8790-8839.

10. Zhang, B.; Tan, R.; Yang, L.; Zheng, J.; Zhang, K.; Zhang, K.; Mo, S.; Lin, Z. Mechanisms and properties of ion-transport in inorganic solid electrolytes. *Energy Storage Mater.* **2018,** *10,* 139-159.

11. Waetzig, K.; Rost, A.; Heubner, C.; Coeler, M.; Nikolowski, K.; Wolter, M.; Schilm, J. Synthesis and sintering of $Li_{1.3}Al_{0.3}Ti_{1.7}(PO_4)_3$ (LATP) electrolyte for ceramics with improved $Li^+$ conductivity. *J. Alloys Compd.* **2020,** *818,* 153237.

12. Dokko, K.; Hoshina, K.; Nakano, H.; Kanamura, K.; Preparation of $LiMn_2O_4$ thin-film electrode on $Li_{1+x}Al_xTi_{2-x}(PO_4)_3$ NASICON-type solid electrolyte. *J. Power Sources* **2007,** *174,* 1100–1103.

13. Aono, H.; Sugimoto, E.; Sadaoka, Y.; Imanaka, N.; Adachi, Gy. Ionic conductivity of solid electrolytes based on lithium titanium phosphate. *J. Electrochem. Soc.* **1990,** *137,* 1023–1027.

14. Schroeder, M.; Glatthaar, S.; Binder, J. R. Influence of spray granulation on the properties of wet chemically synthesized $Li_{1.3}Ti_{1.7}Al_{0.3}(PO_4)_3$ (LATP) powders. *Solid State Ion.* **2011,** *201,* 49–53.

15. Kobayashi, Y.; Takeuchi, T.; Tabuchi, M.; Ado, K.; Kageyama, H. Ionic conductivity of solid electrolytes based on lithium titanium phosphate. *J. Power Sources* **1999,** *81–82,* 853–858.

16. Arbi, K.; Lazarraga, M. G.; Chehimi, D. B. H.; Ayadi-Trabelsi, M; Rojo, J. M; Sanz, J. Lithium mobility in $Li_{1.2}Ti_{1.8}R_{0.2}(PO_4)_3$ compounds (R = Al, Ga, Sc, In) as followed by NMR and impedance spectroscopy. *Chem. Mater.* **2004,** *16,* 255–262.

17. DeWees, R.; Wang, H. Synthesis and Properties of NaSICON-type LATP and LAGP Solid Electrolytes. *ChemSusChem* **2019,** *12,* 3713 – 3725.

18. Wang, S.; Ben, L; Li, H.; Chen, L. Identifying $Li^+$ ion transport properties of aluminum doped lithium titanium phosphate solid electrolyte at wide temperature range. *Solid State Ion.* **2014,** *268,* 110–116.

19. Arbi, K.; Mandal, S.; Rojo, J. M.; Sanz, J. Dependence of Ionic Conductivity on Composition of Fast Ionic Conductors $Li_{1+x}Ti_{2-x}Al_x(PO_4)_3$, $0 \leq x \leq 0.7$. A Parallel NMR and Electric Impedance Study. *Chem. Mater.* **2002,** *14 (3),* 1091-1097.

20. Xiaoa, W.; Wang, J.; Fan, L.; Zhang, J.; Xifei Li. Recent advances in $Li_{1+x}Al_xTi_{2-x}(PO_4)_3$ solid-state electrolyte for safe lithium batteries. *Energy Storage Mater.* **2019,** *19,* 379–400.

21. Xu, X.; Wen, Z.; Yang, X.; Chen, L. Dense nanostructured solid electrolyte with high Li-ion conductivity by spark plasma sintering technique. *Mater. Res. Bull.* **2008,** *43,* 2334–2341.

22. Yen, P. Y.; Lee, M. L.; Gregory, D. H.; Liu, W. R. Optimization of sintering process on $Li_{1+x}Al_xTi_{2-x}(PO_4)_3$ solid electrolytes for all-solid-state lithium-ion batteries. *Ceram. Int.* **2020,** *46,* 20529–20536.

23. Yana, G.; Yu, S.; Nonemacher, J. F.; Tempel, H.; Kungl, H.; Malzbender, J.; Eichel, R. A.; Krüger, M. Influence of sintering temperature on conductivity and mechanical behavior of the solid electrolyte LATP. *Ceram. Int.* **2019,** *45,* 14697–14703.

24. Hupfer, T.; Bucharsky, E. C.; Schell, K. G.; Hoffmann, M. J. Influence of the secondary phase $LiTiOPO_4$ on the properties of $Li_{1+x}Al_xTi_{2-x}(PO_4)_3$ (x = 0; 0.3). *Solid State Ion.* **2017,** *302,* 49–53.

25. Johnson, P.; Sammes, N.; Imanishi, N.; Takeda, Y.; Yamamoto, O. Effect of microstructure on the conductivity of a NASICON-type lithium ion conductor. *Solid State Ion.* **2011,** *192,* 326–329.

26. Duluard, S.; Paillassa, A.; Puech, L.; Vinatier, P.; Turq, V.; Rozier, P.; Lenormand, P.; Taberna, P. L.; Simon, P.; Ansart, F. Lithium conducting solid electrolyte $Li_{1.3}Al_{0.3}Ti_{1.7}(PO_4)_3$ obtained via solution chemistry. *J. Eur. Ceram. Soc.* **2013,** *33,* 1145-1153.

27. Waetzig, K.; Rost, A.; Langklotz, U.; Matthey, B.; Schilm, J. An explanation of the microcrack formation in $Li_{1.3}Al_{0.3}Ti_{1.7}(PO_4)_3$ ceramics. *J. Eur. Ceram. Soc.* **2016,** *36,* 1995-2001.

28. Jackman, S. D.; Cutler, R. A. Effect of microcracking on ionic conductivity in LATP. *J. Power Sources* **2012,** *218,* 65-72.

29. Gellert, M.; Dashjav, E.; Grüner, D.; Ma, Q.; Tietz, F. Compatibility study of oxide and olivine cathode materials with lithium aluminum titanium phosphate. *Ionics* **2018,** *24,* 1001–1006.

30. Albetran, H., O'Connor, B. H., & Low, I. M. Effect of calcination on band gaps for electrospun titania nanofibers heated in air–argon mixtures. *Mater Des.* **2016**, 92, 480-485.

31. Huang, C. Y.; Agrawal, D. K.; McKinstry, H. A. Thermal expansion behaviour of $M'Ti_2P_3O_{12}$ (M'-Li, Na, K, Cs) and $M''Ti_4P_6O_{24}$ (M''=Mg, Ca, Sr, Ba) compounds. *J. Mater. Sci.* **1995,** *30,* 3509-3514.

32. Woodcock, D. A.; Lightfoot, P. Comparison of the structural behaviour of the low thermal expansion NZP phases $MTi_2(PO_4)_3$ (M=Li, Na, K). *J. Mater. Chem.* **1999,** *9,* 2907-2911.

33. Bucharsky, E. C.; Schell, K. G.; Hintennach, A.; Hoffmann, M. J. Preparation and characterization of sol–gel derived high lithium ion conductive NZP-type ceramics $Li_{1+x}Al_xTi_{2-x}(PO_4)_3$. *Solid State Ion.* **2015,** *274,* 77–82.

34. Kleitz, M., Dessemond, L., & Steil, M. C. Model for ion-blocking at internal interfaces in zirconias. *Solid State Ion.* **1995**, *75,* 107-115.

35. Rettenwander, D., Welzl, A., Pristat, S., Tietz, F., Taibl, S., Redhammer, G. J., & Fleig, J. A microcontact impedance study on NASICON-type $Li_{1+x}Al_xTi_{2-x}(PO_4)_3$ ($0 \leq x \leq 0.5$) single crystals. *J. Mater. Chem. A* **2016**, *4(4)*, 1506-1513.

36. Aono, H.; Sugimoto, E.; Sadaoka, Y.; Imanaka, N.; Adachi, G.-y. DC Conductivity of $Li_{1.3}Al_{0.3}Ti_{1.7}(PO_4)_3$ Ceramic with Li Electrodes. *Chem. Lett.* **1991,** *20,* 1567−1570.

37. Liu, Y.; Sun, Q.; Zhao, Y.; Wang, B.; Kaghazchi, P.; Adair, K. R.; Li, R.; Zhang, C.; Liu, J.; Kuo, L. Y.; Hu, Y.; Sham, T. K.; Zhang, L.; Yang, R.; Lu, S.; Song, X.; Sun, X.; Stabilizing the Interface of NASICON Solid Electrolyte against Li Metal with Atomic Layer Deposition. *ACS Appl. Mater. Interfaces* **2018,** *10,* 31240−31248.

38. Zhu, Y.; He, X.; Mo, Y. Origin of Outstanding Stability in the Lithium Solid Electrolyte Materials: Insights from Thermodynamic Analyses Based on First-Principles Calculations. *ACS Appl. Mater. Interfaces* **2015,** *7,* 23685−23693.

39. Liu, J.; Liu, T.; Pu, Y.; Guan, M.; Tang, Z.; Ding, F.; Xu, Z.; Li, Y. Facile synthesis of NASICON-type $Li_{1.3}Al_{0.3}Ti_{1.7}(PO_4)_3$ solid electrolyte and its application for enhanced cyclic performance in lithium ion batteries through the introduction of an artificial $Li_3PO_4$ SEI layer. *RSC Adv.* **2017,** *7,* 46545–46552.

40. Nairn, K. M.; Best, A. S.; Newman, P. J.; MacFarlane, D. R.; Forsyth, M. Ceramic-Polymer Interface in Composite Electrolytes of Lithium Aluminium Titanium Phosphate and Polyetherurethane Polymer Electrolyte. *Solid State Ion.* **1999,** *121,* 115−119.

41. Zhou, W.; Wang, S.; Li, Y.; Xin, S.; Manthiram, A.; Goodenough, J. B. Plating a Dendrite-Free Lithium Anode with a Polymer/Ceramic/Polymer Sandwich Electrolyte. *J. Am. Chem. Soc.* **2016,** *138,* 9385−9388.

42. Li, L.; Zhang, Z.; Luo, L.; You, R.; Jiao, J.; Huang, W.; Wang, J.; Li, C.; Han, X.; Chen, S. Enhancing the interface stability of $Li_{1.3}Al_{0.3}Ti_{1.7}(PO_4)_3$ and lithium metal by amorphous Li1.5Al0.5Ge1.5(PO4)3 modification. *Ionics* **2020,** *26*, 3815–3821.

## Graphical Abstract